

## Three-dimensional odorant concentration measurements around actively tracking blue crabs

Brian D. Dickman<sup>1</sup>, Donald R. Webster<sup>1\*</sup>, Jennifer L. Page<sup>2,3</sup>, and Marc J. Weissburg<sup>2</sup>

<sup>1</sup>School of Civil & Environmental Engineering, Georgia Institute of Technology, Atlanta, GA, USA 30332-0355

<sup>2</sup>School of Biology, Georgia Institute of Technology, Atlanta, GA, USA 30332-0230

<sup>3</sup>Previously published as J.L. Jackson

### Abstract

Blue crabs (*Callinectes sapidus*) and other aquatic organisms locate food and mates by tracking turbulent odorant plumes. The odorant concentration fluctuates unpredictably due to turbulent transport, and many characteristics of the fluctuation pattern have been hypothesized as useful cues for orienting to the odorant source. To make a direct linkage between tracking behavior and odorant signal properties, we developed a laser-induced fluorescence measurement system to quantify the instantaneous three-dimensional (3D) concentration field surrounding actively tracking blue crabs. The data suggest a connection between upstream walking speed and bursts of odorant concentration arriving at the antennule chemosensors, which are located near the mouth region. Specifically, we note rapid upstream walking speed when high concentration bursts arrive at the antennules location and a decrease in upstream walking speed in the absence of odorant filaments near the antennules. Additionally, we note transverse crab movements in apparent response to the transverse distribution of the odorant concentration field. Specifically, asymmetry of the odorant concentration distribution at the elevation of the leg chemosensors is associated with subsequent crab position adjustments in the transverse direction. The methods described here allow for powerful and direct tests of chemosensory navigation strategies in blue crabs, as well as other macroscopic aquatic animals.

### Introduction

Organisms have developed a wide variety of strategies to find the source of an odor due to the necessity of locating critical odor sources (e.g., food or mates). Behavioral studies on many organisms have been used to investigate tracking mechanisms that animals use to find resources in turbulent environments (reviewed in Weissburg 2000; Vickers 2000; Zimmer and Butman 2000; Moore and Crimaldi 2004; Koehl 2006). Tracking behavior experiments generally consist of placing an animal in a controlled flow environment, releasing an attractant odorant upstream or upwind, and observing subsequent tracking behavior. These studies reveal much about behavioral response and subsequent locomotory patterns, yet offer little more than a qualitative idea of the olfactory stimulus expe-

rienced by the tracking organism. Previous studies have attempted to determine the relationship between stimulus and behavioral response by examining general properties of plume structure and correlating these general plume properties to tracking behavior under similar flow conditions (e.g., crustaceans: Jackson et al. 2007 and references therein; insects: Elkinton et al. 1984; Murlis et al. 1992). However, these generalizations do not establish the specific plume properties that are essential for organisms to execute a successful track through a turbulent chemical plume. Correlation of the instantaneous plume structure with simultaneous visualization of tracking behavior is necessary to determine the relevant plume properties that govern behavioral decisions during tracking. To accomplish this task, odorant concentration at the location of the olfactory organs must be measured at spatial and temporal scales that are consistent with organism sensing abilities. The measurement technique must also be minimally intrusive because physical probes disturb the flow (and often collect data only at a single point).

The physical characteristics of passive scalar plumes released in the atmosphere or aquatic environments have been measured with a variety of techniques, such as optical methods using smoke as a tracer (Dinar et al. 1988), flame-ionization

\*Corresponding author: E-mail: dwebster@ce.gatech.edu

### Acknowledgments

The authors thank Kimberlee Berkenkamp for assistance with the crab trails and James Bullock for assistance with movie construction. Thanks also to the National Science Foundation for financial support under grants IBN-0321444 and OCE-0424673 to M.J.W. and D.R.W. and for an IGERT fellowship awarded to J.L.P.

detectors (Fackrell and Robins 1982), ion detectors (Jones 1983; Mylne 1993), conductivity probes (Bara et al. 1992), and cold wires (Gulitski et al. 2007). Chemical microprobes also have been used to measure scalar structure in turbulent aquatic plumes relevant to chemosensory foragers (e.g., Moore and Atema 1991). The results of these and other studies have provided insight to the navigational environments that organisms experience (e.g., Murlis et al. 1992). While these methods may resolve scalar structure, many are impossible or impractical to apply in conjunction with behavior, given the large size of the sensors or apparatus. Chemical microprobes are the most promising technology, given their small size and spatial and temporal sampling characteristics; however, they may be of limited utility in settings requiring multiple measurement locations. Further, gathering simultaneous information at neighboring points requires an array of probes, potentially altering the dynamics of the flow.

Laser-induced fluorescence (LIF) permits nonintrusive quantitative measurement of instantaneous concentration fields (Koochesfahani and Dimotakis 1985; Crimaldi 2008), although the technique is limited to controlled laboratory settings. Laser-induced fluorescence involves the use of low concentrations of a tracer dye, or fluorophore, which excites at a molecular level when exposed to laser light. The odorant plume is nearly identical to that of the fluorophore as long as the odorant and tracer diffuse at the same rate and decay minimally. In recent years, the planar laser-induced fluorescence (PLIF) technique has been employed to quantify the concentration distribution in turbulent odorant plumes with parameters of ecological relevance (Crimaldi et al. 2002b; Webster et al. 2003; Rahman and Webster 2005).

A logical progression is to combine laser-induced fluorescence with an actively tracking organism to directly correlate navigational behavior with odorant concentration at olfactory organs. However, combining traditional PLIF with organism studies has been restricted by many factors. Shadowing of the laser by portions of the organism body can create gaps in the concentration time record at shaded chemosensors. Animals generally track while shifting the vertical location of olfactory organs (by moving up and down or by antennule flicking), which causes them to move in and out of any given planar measurement field. Further, the olfactory systems of some arthropods, such as blue crabs, are not limited to a single location, such as the antennules, but are distributed across the animal's body at multiple elevations. In addition, the intense laser light used in PLIF can disorient animals and thereby disrupt tracking. For many of these reasons, simultaneous PLIF measurements during tracking has been restricted to one study on the stomatopod (*Hemisquilla ensiguera californica*), where analysis was focused on chemical cue structure at the pair of antennules, each with a central aesthetasc array (Mead et al. 2003). Planar laser-induced fluorescence enabled the measurement of the concentration field along the aesthetasc array for wave-driven and unidirectional flow. Only seven

plume tracks (out of ninety) could be used in the analysis due to problems associated with coordinating PLIF with an actively tracking animal. Nevertheless, the measurements provided insights into potential information content of turbulent plumes that would have been difficult to obtain with other methods (Mead et al. 2003).

The objective of this article is to describe a three-dimensional laser-induced fluorescence (3DLIF) system for use in a seawater laboratory flume with an actively tracking blue crab, *Callinectes sapidus*. This system generates a three-dimensional, time-resolved measurement to provide a comprehensive and useful characterization of odorant plume structure as an animal tracks to a source. *Callinectes sapidus* has at least two types of chemosensory organs that are responsible for orientation. Odor stimulus at the antennules (located near the mouth region) apparently is responsible for maintaining upstream movement (Keller et al. 2003; Jackson et al. 2007). Chemosensors on the legs are spatially separated and allow perception of a contrast between sides of the crab's body. Turns are believed to occur when a bilateral contrast is sensed, a response referred to as tropotaxis. Since sampling occurs at multiple elevations and transverse locations, any attempt to quantify the stimulus patterns experienced by a tracking blue crab would necessarily have to include measurements from more than a single plane.

Data collected from this system allow us to examine the relationships between signal input and behavioral output during chemosensory orientation, which is necessary to test hypotheses about orientation mechanisms in any system. In particular, studying tracking behavior in aquatic environments will provide insights into the tracking behavior of terrestrial organisms such as insects following pheromone trails (Mafra-Neto and Cardé 1994; Vickers and Baker 1994), as well as other aquatic organisms. Rapid movement through an odorant plume is a common trait between blue crabs (i.e., aquatic tracker) and moths (i.e., terrestrial tracker) as they both have to encode information from highly intermittent odorant filaments relatively quickly in order to find an odorant source. Organisms in both environments orient to the prevailing flow conditions to guide their tracking behavior and face a tracking problem in three-dimensions, providing additional common mechanisms between the different fluid realms. We present initial examples of data that associate spatial and temporal properties of the concentration field with movements of blue crabs tracking to an odorant source as a step towards a deeper understanding of tracking mechanisms of organisms following turbulent plumes in any environment.

### Materials and procedures

*Laboratory facility*—Experiments were performed in the environmental fluid mechanics laboratory at the Georgia Institute of Technology in Atlanta, Georgia, USA. The seawater flume dimensions were 0.76 m wide by 13.5 m long with a level bed and transparent polyacrylic sidewalls. The transparent sidewalls in the test section allowed optical access and the use

of LIF. A polyacrylic sheet was suspended at the water surface in order to eliminate refraction effects from small waves on the water surface during experiments and calibration. Flow conditions replicated those typically found in blue crab tidal habitats (Finelli et al. 1999; Smeed and Weissburg 2006), and the channel bed was lined with fine sand ( $d_{50} = 1$  mm). A simple rectangular weir fixed the flow depth at 21.2 cm to maintain a mean flow velocity of  $50 \text{ mm s}^{-1}$ , which yielded a boundary layer with roughness Reynolds number of approximately 3 and a wall shear velocity ( $u^*$ ) of  $3.0 \text{ mm s}^{-1}$  (Jackson et al. 2007).

A mixture of chemical attractant and a trace amount of Rhodamine 6G was released iso-kinetically (without momentum relative to the flow) through a 4.2 mm diameter nozzle located upstream of the test section. The release centerline was positioned 25 mm above the substrate, which is within the inertial region of the turbulent boundary layer. A streamlined fairing on the nozzle limited the wake perturbation. A coordinate system was defined with the origin located at the top of the sand directly below the nozzle tip with positive  $x$  in the downstream direction,  $y$  in the transverse (cross-stream) direction with positive values on the side of the incoming laser beam, and positive  $z$  in the upward vertical direction.

**3DLIF System**—Laser-induced fluorescence is an established technique used to measure chemical concentration in a flow in a relatively nonintrusive manner (Crimaldi 2008). The technique has been used extensively and the LIF system for this study is similar to those developed by previous investigators (e.g., Crimaldi and Koseff 2001; Webster et al. 2003). Three-dimensional LIF is an experimental technique that builds upon PLIF and can be used to measure the nearly instantaneous three-dimensional concentration field (Tian and Roberts 2003; Van Vliet et al. 2004). The 3DLIF system was constructed adjacent to the test section of the seawater flume (see Figs. 1 and 2). Rhodamine 6G, a commercially available

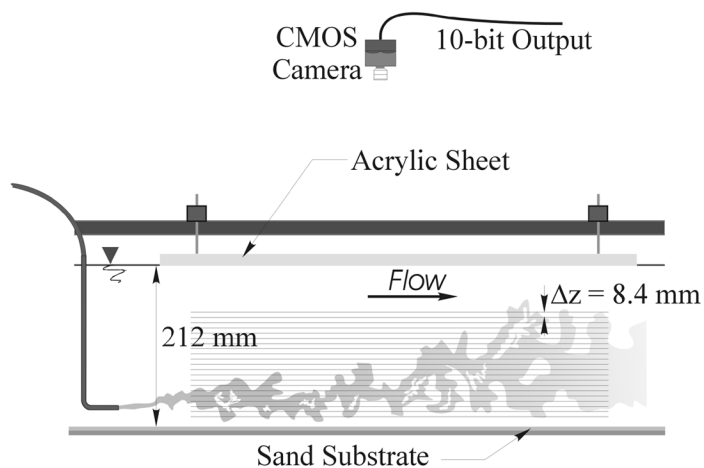


**Fig. 1.** Experimental setup for the 3DLIF system, as seen from the side of the flume. The horizontal lines represent the sequential locations of the laser scan.

organic dye, was chosen as the fluorophore due to its resistance to photobleaching (Crimaldi 1997; Larsen and Crimaldi 2006) and peak absorption wavelength of 530 nm, which is close to the laser light wavelength. The peak fluorescent emission wavelength is near 560 nm (Arcoumanis et al. 1990). The Rhodamine 6G solution was added to an attractant solution to serve as a measurable proxy for the relative concentration of the stimulant solution that elicits orientation by freely moving blue crabs. Therefore, we report chemical concentration relative to the initial source concentration,  $C_0$ .

The attractant had neutral buoyancy and was created by soaking 2.21 g of previously frozen shrimp per liter of seawater (taken from the flume sump) for 1 h. This general preparation has been used in many behavioral assays involving aquatic organisms and, in particular, blue crabs have effectively tracked sources of chemical exudates of shrimp in previous behavioral trials (Keller et al. 2003; Jackson et al. 2007). The specific concentration of stimulus was chosen as a value in the middle of the dose-response range of blue crabs. This created an odorant plume that crabs could follow under continuous, iso-kinetic release conditions, but where tracking was not so effective as to obscure relationships between the stimulus properties and the resulting behavioral response. The addition of Rhodamine 6G to the shrimp exudates revealed no significant differences in blue crab behavior trials. The attractant-Rhodamine 6G solution was nonreactive within the test section and was transported passively by the flow. The Schmidt number of Rhodamine 6G is approximately 1250, which is of the same order of magnitude of the Schmidt

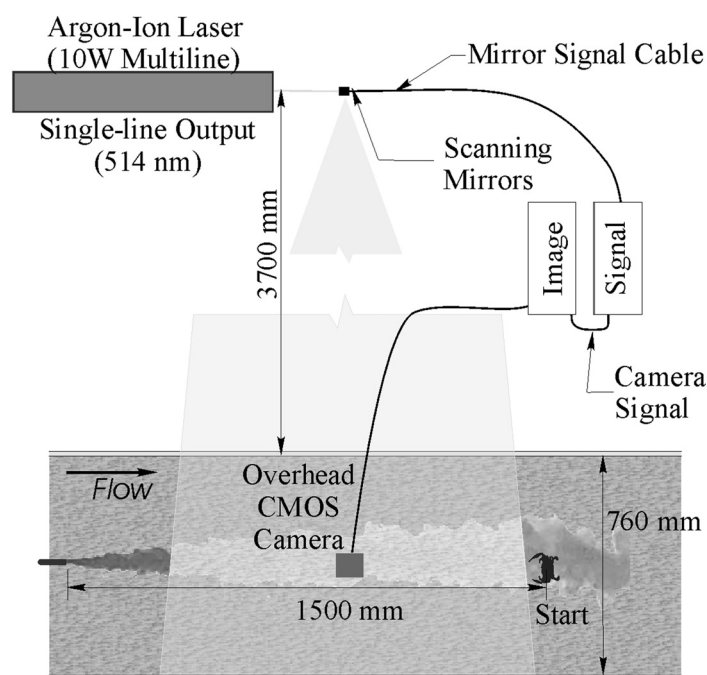


**Fig. 2.** Arrangement for the 3DLIF system and overhead view of measurement area.

number of the chemical exudates, so the dye and attractant filaments can be assumed coincident.

An Argon-ion laser (Coherent Innova 100-10) provided illumination at a power level of 5.0 W and a wavelength of 514 nm. A 4 m focal length lens reduced the  $1/e^2$  diameter of the laser beam to approximately 1 mm at flume centerline. The beam was scanned across the measurement section by a pair of orthogonally mounted mirrors attached to galvanometers. The horizontal mirror progressively advanced the laser beam in the horizontal direction, thereby effectively creating a two-dimensional sheet of light. At the end of the horizontal laser scan, the vertical mirror shifted the beam a small vertical distance prior to the initiation of the next horizontal scan, thereby sequentially illuminating a three-dimensional measurement volume. Fluorescence emitted by the dye during each horizontal scan was collected by an overhead digital camera. The measurement sequence included 20 horizontal scans separated vertically by approximately 8.4 mm with the lowest and highest scan positions located at 0.5 cm and 16.5 cm above the channel substrate at flume centerline, respectively. The height of the lowest plane was chosen to enable sampling at the approximate level of the leg chemosensors of *C. sapidus* and the highest plane was chosen to contain the upper extent of the plume within the measurement volume.

For an iso-kinetic plume released into an unbounded moving turbulent fluid, the time-averaged concentration ( $\bar{c}$ ) follows a theoretical decay that is inversely proportional to distance downstream from the point source (i.e.,  $\bar{c} \propto x^{-1}$ ) (Albertson et al. 1950). The power law decrease assumes that turbulence is isotropic and that  $x$  is sufficiently downstream from the source for all ambient eddy sizes to be involved in mixing. The resulting fluorescence intensity under uniform illumination decreases significantly with distance from the source, due to the decrease in concentration. Therefore, images covering 1 m or more of the plume become dim at the downstream end of the image with poor signal-to-noise ratio. Consequently, we used a power law control signal to the mirrors to increase the beam residence time in the downstream (low concentration) region relative to that in the upstream (high concentration) region. Webster et al. (2003) describe the use of nonuniform angular speeds of the horizontal mirror in PLIF experiments for flow and release conditions similar to this study. In the current experiments, a power law with an exponent of  $n = 0.75$  was used to control the sweep rate and yielded the most uniform images (i.e., the voltage signal sent to the mirror was

$$E = E_o + (E_1 - E_o) \left( \frac{t}{T} \right)^{1/(n+1)} \quad (1)$$

where  $E_o$  and  $E_1$  correspond to the start and end voltages, respectively, and  $T$  is the period of the horizontal sweep).

**3DLIF data collection and resolution**—The overhead camera (Mikrotron model MC1302) had a  $1280 \times 1024$  array of complementary metal-oxide semiconductor (CMOS) sensors

with a pixel depth of 10 bits (0 to 1023 grayscale value). The pixel array size used during experiments was 1030 streamwise by 480 transverse. These dimensions were set by calibration limitations and pixel sensitivity concerns near the array perimeter. An optical filter (Tiffen Orange 21 with a cutoff wavelength of approximately 560 nm) and a standard hot mirror were placed over the camera lens to pass fluoresced light while eliminating scattered laser light and protecting the camera sensors. A Fujinon 12.5-mm focal length lens was used to achieve a 1 mm pixel resolution at an elevation of 50 mm above the channel substrate. The highest lens aperture (f-stop of 1.4) was used to maximize the amount of light arriving at each CMOS sensor. The resulting depth of field allowed an adequate level of focus for each of the 20 scan elevations.

The camera collected images at 100 frames per second and coordinated with the scanning mirrors through a National Instruments multifunction input/output (I/O) board (PCI-MIO-16E-4) programmed with LabView software. Scanning was initiated after a transistor-to-transistor logic (TTL) signal was transmitted from the camera to the I/O board (i.e., the camera acted as the timing master). A proprietary computer system developed by IO Industries Inc. (London, Ontario, Canada) collected camera image data via Video Savant software with an array of six 36.6-gigabyte hard drives through a CameraLink cable with a data rate of 66 MHz (10 bits per clock cycle on 2 channels). As configured, the recording system had the capacity to collect continuous data for 14 min. The resulting 3DLIF collection rate was slightly less than 5 Hz (i.e., 100 fps/20 planes), as timing differences between the National Instruments board and the IO Industries framegrabbers resulted in a blank frame at the end of each 3DLIF volume set (i.e., the 20 planes required 0.21 s to collect). The laser beam rested to the side of the recording area during collection of the blank frames, which were removed during post-processing of the image files.

The 3DLIF resolution (approximately 1 mm in each plane) for this study was chosen to be greater than the Batchelor scale and is a compromise between matching the presumptive sensor resolution of blue crabs and recording a field of view sufficiently large to contain a tracking crab. The Batchelor scale is a measure of the scale of the smallest spatial variation in the concentration field for large Schmidt numbers (Batchelor 1959), and is on the order of 0.03 mm for this study. Although there are sensors on many body regions, major groups of crustacean sensilla are concentrated at certain locations, such as along the antennules and on portions of the legs. These chemosensory organs contain sensor arrays that typically have dimensions on the order of millimeters, but the effective scalar-detecting resolution of aquatic crustaceans is an open question. Although the size of an individual aesthetasc is smaller than the Batchelor scale, chemical information is believed to be smeared by motion of the appendages (e.g., flicking of the antennules, Schmitt and Ache 1979; Leonard et al. 1994; Koehl et al. 2001) and neurological pooling. Current behavioral studies are not sufficient to resolve whether

sub-millimeter scale information is used in orientation, but do indicate that spatial comparisons between different chemosensory appendages are critical for plume tracking (Zimmer Faust et al. 1995; Jackson et al. 2007). Temporal sampling capabilities also limit detection of small-scale odorant filament structure. The chemosensory response rate for crustaceans is believed to be in the range of 5 Hz (Gomez and Atema 1996), which is too slow to resolve the time-scales of concentration fluctuations (Webster and Weissburg 2001). Further, Crimaldi et al. (2002a) examined the influence of sensor size and sampling frequency on the signal pattern gathered by a virtual antennule in a turbulent odorant plume in the laboratory. Their results indicate that signal intermittency is nearly independent of sensor size for sampling frequencies in the range of 5 Hz. In summary, the data collection rate (~ 5 Hz) and pixel resolution (~ 1 mm) chosen for this study agree well with temporal and spatial sampling resolutions known to provide information in our test organism, *C. sapidus*.

**LIF Calibration**—System calibration is necessary to generate meaningful concentration data from LIF. Calibration consisted of scanning the laser through seawater taken from the flume with fixed, uniform concentrations of Rhodamine 6G. A transparent polyacrylic tank was centered in the flume and filled with a known volume of seawater. Flow depth in the flume was set to the depth used in subsequent experiments (21.2 cm) to include attenuation effects due to seawater between the flume and calibration tank walls. A weighed amount of Rhodamine 6G was mixed uniformly into the seawater in the tank and laser scanning was initiated at the same positions used during data collection. The fluorescent signal was collected for 100 frames at each laser scan elevation using 10 to 12 concentration levels from 0 to 100  $\mu\text{g L}^{-1}$ .

The calibration images were corrected for attenuation using the in-situ estimate of the extinction coefficient and the laser distance to each pixel. With attenuation effects removed (described below), a pixel by pixel calibration was performed. For Rhodamine 6G concentrations below 100  $\mu\text{g L}^{-1}$ , the calibration resulted in a linear relationship between concentration and the camera pixel intensity (Ferrier et al. 1993):  $c = \alpha_c I$ , where  $I$  is the grayscale value of the camera pixel and  $\alpha_c$  is a constant of proportionality including effects of laser power, laser scan rate, nonuniformities in the flume sidewalls, and the efficiency and sensitivity of the camera pixels.  $\alpha_c$  was determined for each individual pixel from a least-squares linear fit of concentration versus camera pixel value.

Attenuation of laser intensity occurs due to absorption and scattering when the beam passes through a fluid medium. The decrease in power is assumed to follow the Bouguer-Lambert-Beer law,  $P(\xi) = P_0 e^{-\beta \xi}$ , where  $P(\xi)$  is the laser power at a distance  $\xi$  within the medium,  $P_0$  is the initial laser power at  $\xi = 0$ , and  $\beta$  is an attenuation coefficient. The attenuation coefficient is not generally constant with varying concentration and can be derived from three variables:  $\beta = \beta_{sw} + \lambda c$ , where  $\beta_{sw}$  is a base attenuation coefficient due to attenuation from

seawater and other effects,  $\lambda$  is the extinction coefficient, and  $c$  is the concentration of Rhodamine 6G. The extinction coefficient for Rhodamine 6G to laser light at 514 nm has been reported as  $-0.00023 \mu\text{g}^{-1} \text{L cm}^{-1}$  by Ferrier et al. (1993) and  $-0.00021 \mu\text{g}^{-1} \text{L cm}^{-1}$  by Brackmann (2000). Rhodamine 6G is available in different forms from various commercial vendors and the extinction coefficient is likely to vary.

An in-situ attenuation coefficient was calculated from the calibration data for this study. Attenuation was determined from examining the decrease in beam power as indicated by decreasing pixel intensity (10-bit value) for each calibration concentration. A column of pixels collinearly aligned with the beam and perpendicular to the flume centerline was analyzed. To isolate attenuation effects, intensity values within the pixel column were corrected for beam residence time and differences in pixel sensitivity. Laser light reflected from a scanning mirror passes through the integration area of a camera pixel sensor at speeds dependent upon radial distance from the mirrors and horizontal beam angle (Crimaldi and Koseff 2001). The residence time correction for small horizontal beam angles is simply the ratio of the radial distances of a given pixel and the front of the calibration tank. Pixel sensitivity was determined by finding the most sensitive pixel, i.e., the pixel with the greatest difference in digital output between a white and black level image. Following the procedure of Tian and Roberts (2003), the remaining pixels were normalized to the maximum. Each pixel intensity value within the collinear column was corrected using a normalization coefficient from the black and white level images. The normalization procedure allowed the decrease in power to be related directly to recorded fluorescence intensity by removing the effects of individual pixel sensitivity. Differences in contiguous pixel sensitivity were further reduced by averaging a row of 5 pixels centered on the laser centerline, i.e., the column was approximately 5 mm wide. The 3DLIF scan elevation closest to the mirror level was used to remove effects of vertical beam angle on distance traveled. An average of the first 5 pixel values, covering a distance of 5 mm into the calibration tank, was employed as a base power level  $P_0$ . Plots of corrected pixel intensity versus distance through the calibration tank displayed an exponential decay as expected (see Fig. 3). The extinction and base attenuation coefficients were calculated by fitting the log-transformed data to a least-squares fit line. The resulting extinction and base attenuation coefficients were  $-0.00024 \mu\text{g}^{-1} \text{L cm}^{-1}$  and  $-0.004 \text{cm}^{-1}$ , respectively.

A grid with spacing of 50 mm by 50 mm was placed in the flume to determine magnification and refraction effects. Images of the grid were taken when located at the approximate elevations of the lowest scan and the water surface. The effects of refraction and magnification at each elevation of the 3DLIF planes were corrected based on the collected target images by interpolation to intermediate elevations.

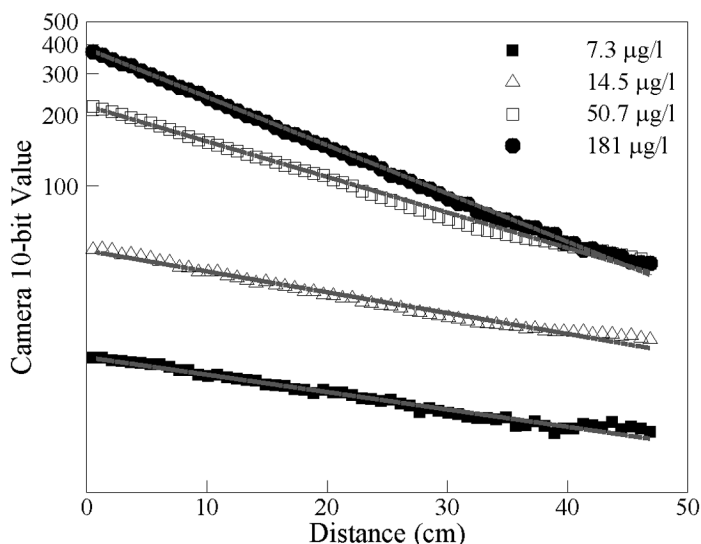


**Fig. 3.** Decrease in recorded intensity through the calibration tank on semi-log plot for 4 sample concentrations. The camera intensity values have been corrected for laser residence time and individual pixel response. Every tenth data point and best-fit lines are shown.

Finally, our data analysis corrected for noise present in the recorded camera signal. The minimum grayscale value  $I_{\min}$  for a single pixel typically fluctuated by roughly 6 to 8 grayscale units when recording a black-level image. The noise was quantified by determining the maximum fluctuation  $\Delta I_{BL}$  for a sequence of 500 frames. Grayscale values below a threshold equal to the minimum plus the maximum fluctuation (i.e.,  $I_{\text{thresh}} = I_{\min} + \Delta I_{BL}$ ) were set to zero concentration during filtering of crab track images. For a typical pixel,  $I_{\min}$  and  $\Delta I_{BL}$  were approximately 28 and 8, respectively, compared to a total grayscale depth of 1024.

As described above, systematic errors were minimized by performing the in-situ pixel by pixel calibration for each LIF plane with constant laser power prior to collecting experimental data and ensuring a linear relationship between pixel intensity and fluorophore concentration. In addition, our measurement uncertainty analysis included consideration of thermal blooming (Wang and Fiedler 2000), lens vignette (Tian and Roberts 2003), photobleaching (Crimaldi 1997; Larsen and Crimaldi 2006), local pH or the interaction of the fluorophore with other chemical species, and other effects discussed above. The resulting estimate of uncertainty in the concentration measurements is  $\pm 3\%$ .

*Integrating biological and physical visualizations*—Blue crabs used in the 3DLIF trials were either collected from Wassaw Sound in Georgia, USA, or purchased from Gulf Specimen Marine Laboratory in Panacea, Florida, USA. The animals were stored in artificial seawater tanks interconnected through a filtered recirculating system and were fed a diet of previously frozen shrimp.

The purpose of performing 3DLIF experiments in conjunction with animal observations is to determine the instantaneous concentration field experienced by the tracking

organism as it approaches a source, hence natural behavior of the animal is required. Unfortunately, blue crabs demonstrated an adverse reaction to intense green laser light. This effect was corrected by reversibly blindfolding the crabs with electrical heat shrink wrap. Blue crabs were permitted to acclimate in the laboratory storage tanks for 48 h prior to blindfolding, and for a minimum of 48 h after blindfolding prior to performing behavior trials. Preliminary experiments indicated that tracking behavior of blindfolded crabs was not significantly different than the behavior of un-blindfolded crabs. This conclusion is supported by a paired  $t$  test assuming equal variances (net-to-gross-displacement-ratio (path linearity) equaled  $0.856 \pm 0.144$  (mean  $\pm$  SD) and  $0.814 \pm 0.101$  for untreated and blindfolded crabs, respectively;  $p = 0.44$ ,  $N = 20, 13$ , respectively; walking speed equaled  $7.394 \pm 2.010 \text{ cm s}^{-1}$  and  $5.713 \pm 2.612 \text{ cm s}^{-1}$  for untreated and blindfolded crabs, respectively;  $p = 0.14$ ,  $N = 20, 13$ , respectively). These values are comparable with those observed over many experiments with blue crabs in similar behavioral trials (Weissburg and Dusenbery 2002; Keller et al. 2003; Jackson et al. 2007). Percent success of crabs with blindfolds was again similar to crabs without blindfolds with untreated crabs achieving 40% success (see Jackson et al. 2007) and blindfolded crabs achieving 46% success of finding the stimulus ( $N = 6$  out of 13). Crabs typically removed the blindfolds (using their claws) within a few days after the experimental trials with no identifiable adverse effects of the blindfolding procedure.

Crab kinematic data were calculated by following two light-emitting diodes (LEDs) in a small backpack attached to the crab carapace. The coordinates of the marker lights were located by finding the center of the bright recorded light in the 3DLIF image. During post-processing, the trajectory of the marker lights was examined for validity by visually comparing the trajectory with the raw image data. Crab velocity and acceleration in each coordinate direction and crab angle with respect to the flume centerline were calculated based on the two light locations (time period of approximately every 0.2 s).

The flume area was darkened during trials to increase the contrast of the emitted light from the fluorescent dye and the backpack lights compared to the background. The crab was acclimated in a cage at the downstream end of the test arena for 10 min. The release of the odorant and fluorescent dye mixture was initiated during this acclimation period to ensure that a developed plume was present for both the acclimation and trial periods. Once the cage door was raised, the crab was given 10 min to initiate tracking by exiting the cage and an additional 10 min to complete its motion across the test section once it departed the cage. The crab either moved through the test section and missed or found the odorant source within this time period, or remained stationary at the downstream edge of the test section for the entire time period. No animal was in the process of tracking at the end of the observation period.

## Assessment

**Quantifying the concentration field and crab kinematics**—We have collected simultaneous odorant concentration and blue crab kinematic data for over 55 successful tracks to the point source. Two typical tracks are presented and discussed here to demonstrate the effectiveness of the measurement technique and its utility in examining chemosensory orientation. Figs. 4 and 5 are example concentration fields of two successful tracks (corresponding movie sequences are shown in the Appendix, AVI1 and AVI2). The panels correspond to data collected in planes located at 0.5 cm and 7.2 cm above the sand substrate, which were chosen as representative of the concentration fields experienced by the leg chemosensors and antennules, respectively. The concentration landscape differs significantly between the lower and upper elevations for both of these examples. In particular, there are fewer filaments present in the upper elevation plane.

Previous behavioral trails and computer simulations have suggested the function and importance of various blue crab chemosensory organs. Based on deafferentation trials, Keller et al. (2003) developed the hypothesis that blue crabs used chemosensors located on the antennules to mediate upstream movement. Chemosensors located on the walking appendages facilitate steering and improved orientation with respect to the plume, potentially through bilateral contrast across the crab's body (Weissburg and Dusenbery 2002; Keller et al. 2003). Hence, the 3DLIF data collected for this study focused on evaluating concentration data from two primary locations around the tracking crab: near the antennule region and near the walking appendage chemosensors.

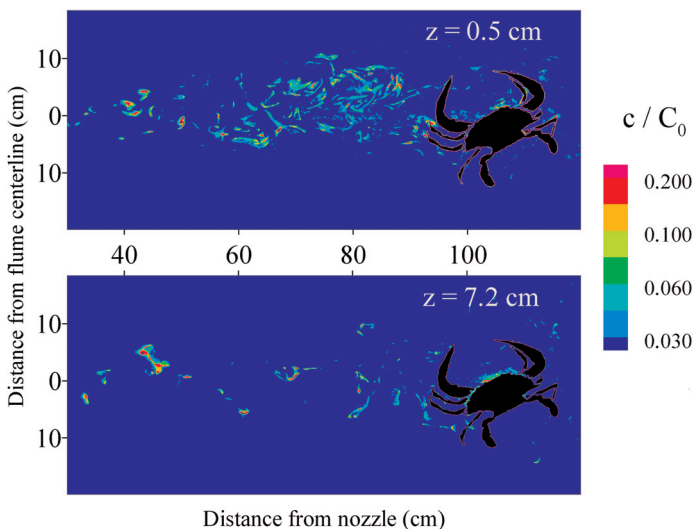


**Fig. 4.** Example concentration field measurements around an actively tracking blue crab for a successful search (crab label 1364L). Concentration fields for two elevations are shown,  $z = 0.5$  cm and  $z = 7.2$  cm, corresponding to the approximate elevation of the chemosensors on the walking appendages and the antennules, respectively. A movie sequence of the tracking behavior is available in the Appendix, AVI1.

Despite optical filters on the CMOS camera lens, laser light reflected from the crab carapace and claws was intense enough to be recorded by the camera sensors. Light reflected from the crab body and shadowing effects created a challenge to develop systematic and consistent methods to determine the odorant concentration impinging upon the crab's outer chemosensors. Mead et al. (2003) encountered similar challenges with their PLIF data with tracking mantis shrimp. Descriptions of the procedures employed to extract meaningful sensory data from the 3DLIF fields follow.

**Antennules zone**—Blue crabs generally oriented their body at an angle relative to the flow direction when traveling upstream against a current (Weissburg and Zimmer-Faust 1993; Weissburg et al. 2003). Depending on the crab's chosen orientation relative to the flow (i.e., left facing or right facing), the crab antennules either faced the laser or were obscured in shadows. Useful information could not be extracted from trials in which the crab body shaded the antennules. Hence, measurements of the concentration field combined with behavior observations were limited to those tracks for which the crab body was facing towards the laser. This corresponded to crabs with their left claw leading upstream in the experimental setup shown in Fig. 2. There is no evidence that the orientation of the crab (i.e., left facing or right facing) influenced the tracking behavior or success.

The elevation of the antennules generally changed as crabs lifted or lowered their thorax as they moved upstream. Three-dimensional measurements allowed odorant concentrations around the antennules to be quantified by matching the varying elevation of the antennules with an elevation of a 3DLIF measurement field. For each 3DLIF set, the elevation of the

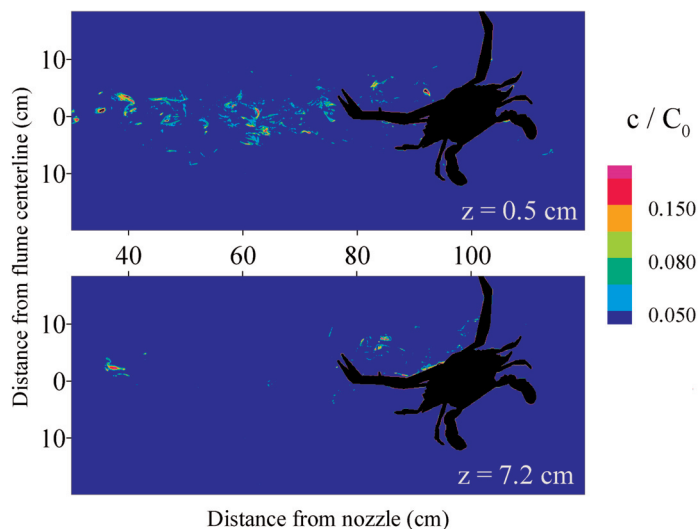


**Fig. 5.** Example concentration field measurements around an actively tracking blue crab for a successful search (crab label 465L). Concentration fields for two elevations are shown,  $z = 0.5$  cm and  $z = 7.2$  cm, corresponding to the approximate elevation of the chemosensors on the walking appendages and the antennules, respectively. A movie sequence of the tracking behavior is available in the Appendix, AVI2.

antennules was estimated through visual inspection of the recorded frames. Each block of images corresponding to the 20 LIF elevations was manually examined, and the image containing reflections from the appropriate carapace region was identified to determine the height of the antennules during that 0.2 s period. As illustrated in Fig. 6, the region used to extract chemosensory data near the antennules was located by geometry in the identified plane. The angle of crab orientation ( $\Psi$ ) was calculated based on the position of the two light-emitting diodes, and a line was projected along the center axis of the crab by bisecting the lights (dashed line in Fig. 6). The sampling region was located along the bisecting line immediately in front of the antennules. The distance from the LED lights to the sampling region varied from 40 to 60 mm, depending on the size of the crab. To determine this distance for each crab specimen, the distance from the LED lights to the mouth region was adjusted until the sampling region fell sufficiently far enough in front of the mouth to avoid creating false filaments based on light reflected off the crab itself. The size of the sampling region was 25 mm by 15 mm, which covered the potential reach of the antennules and included all concentration filaments that may advect past the region between sequential LIF samples.

Two example time records of crab kinematics and odorant concentration within the antennule sampling region during a successful track are shown in Figs. 7 and 8. The variable  $z$  refers to the height of the mouth and antennule region. The crab (label 1364L) shown in Fig. 7 began relatively high in the

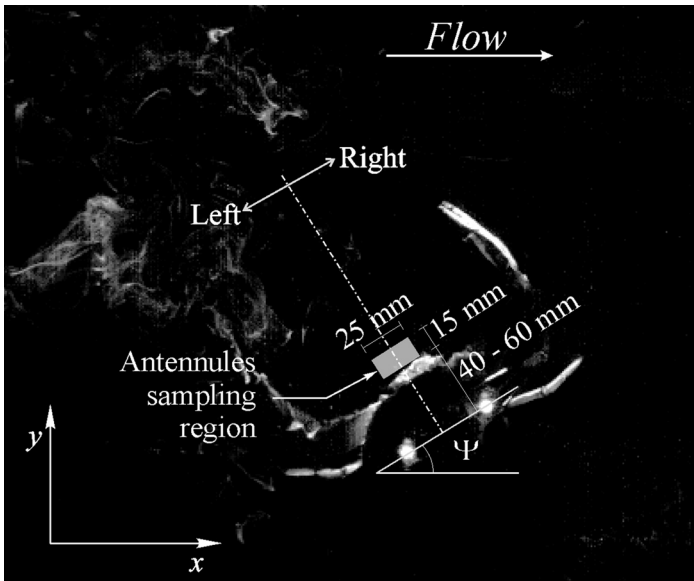


**Fig. 6.** Location of the sampling zone for the crab antennule region. Reflected laser light from the right claw can be seen in the upper right region of the image. Similarly, reflected light from the left claw (although dimmer) is seen in the lower left region of the image. The two bright dots in the lower right region of the image are the light-emitting diodes (LEDs) used to quantify the crab position. Light reflecting from the carapace is observed adjacent to the antennules sampling region.

boundary layer (antennules at  $z = 10$  cm) and then lowered the antennules to between  $z = 6$  and 8 cm. The antennule region received a sequence of odorant bursts during the first 14 s of the time record (labeled in Fig. 7a), and the crab moved rapidly ( $8$  to  $10$  cm  $s^{-1}$ ) upstream during this period (labeled in

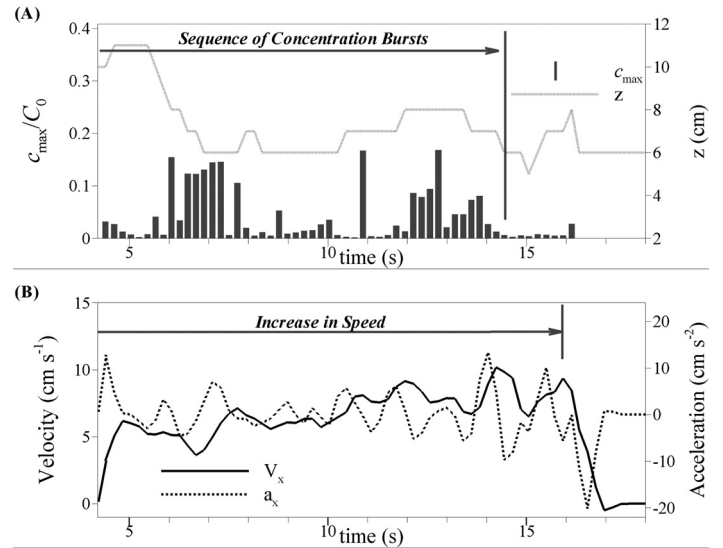


**Fig. 7.** Example concentration and crab kinematic time records for a successful blue crab search (crab label 1364L). Panel A shows the height of the antennules and the normalized concentration data extracted from the antennule sampling region as a function of time during the search.  $c_{max}$  is defined as the maximum concentration sample within the antennule sampling zone and is normalized to the source concentration,  $c_0$ . Panel B shows the crab velocity and acceleration in the upstream direction (i.e.,  $x$  direction).

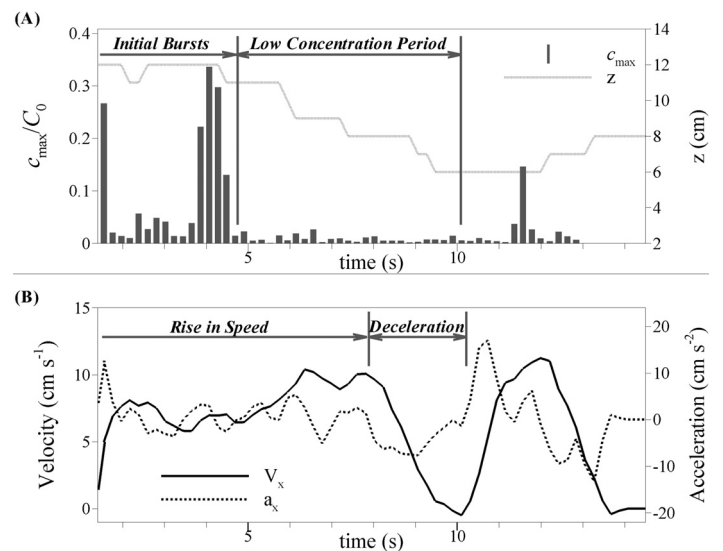


**Fig. 8.** Example concentration and crab kinematic time records for a successful blue crab search (crab label 465L). Panel A shows the height of the antennules and the normalized concentration data extracted from the antennule sampling region as a function of time during the search. Panel B shows the crab velocity and acceleration in the upstream direction (i.e.,  $x$  direction). Parameter definitions are identical to those in Fig. 7.

Fig. 7b for the first 16 s). The concentration signal in the antennules region decreased after 14 s as the crab wandered to the side of the narrow plume structure near the source. Upstream motion was reduced with a negative acceleration around  $t = 16$  s and a rapid decrease in velocity that culminates with the crab coming to a stop ( $V_x = 0$  around  $t = 18$  s).

Crab 465L received several odorant bursts at the antennule region in the first 5 s (labeled in Fig. 8a). Crab velocity in the upstream direction during this period was large and increased until approximately  $t = 7$  s. The crab received minimal chemical stimulus at the antennule region in the period between  $t = 5$  and 10 s. The crab appeared to respond to the lack of chemical stimulus with a decrease in velocity between  $t = 7$  and 10 s. Just after  $t = 10$  s, the crab abruptly accelerated upstream. The time record of concentration does not reveal a stimulus burst in this period, but examination of the concentration field suggests that a strong burst of odorant arrived at the chemosensors on the upstream claw, possibly inducing the motion. Also note that the crab lowers its antennule region in the boundary layer as it proceeds upstream, which is similar to the trend seen in Fig. 7. Our initial analysis suggests that this is a robust pattern associated with a general decrease in the elevation of the center of the plume structure (Page et al. unpubl. data).

**Outer chemosensors**—A contrast between left and right distal chemosensors, usually the legs, could mediate turning towards the interior of the plume (Zimmer-Faust et al. 1995; Webster et al. 2001). We aimed to assess the chemical bias across the crab body to provide insight into whether crabs are responding to spatial asymmetry in the chemical distribution. Direct measurement of odorant concentration at outer chemosensors was not possible due to several experimental constraints. Shadows cast by the carapace, legs, and claws obscured the plume structure close to the legs in many instances. An additional complicating factor was light reflected from the crab, which could not be systematically distinguished from intense fluorescence of high concentration filaments. However, we found that it was possible to estimate the spatial asymmetry of the chemical signal reaching the crab by examining the structure of the approaching plume.

A sampling region projected in front of the crab was used to infer odorant stimulus received by the tracking crab. To prevent interference from the upstream claw, the sampling region was moved upstream by a distance equal to the advection distance over a short time period (i.e., 1 s). Fig. 9 shows an example of the sampling region placement and relative position in time. As shown, the sampling region was moved in space and time sufficiently to prevent false signals from crab appendages, especially the claws. The sampling region size in the streamwise direction was determined by dividing the relative velocity of the crab by the sampling frequency (approximately 4.8 Hz). For example, a crab traveling upstream at  $50 \text{ mm s}^{-1}$  yields a velocity relative to the flow of  $100 \text{ mm s}^{-1}$  and hence the sampling region has a dimension in the streamwise direction of approximately 21 mm (i.e.,  $100 \text{ mm s}^{-1} / 4.8 \text{ Hz}$ ). The sampling region

dimension in the transverse direction matched the width of the crab and varied with crab orientation. For this analysis, the concentration field in the lowest LIF measurement plane was used due to the proximity to the distal appendage chemosensors.

The procedure for extracting the transverse distribution of stimulus is described as follows. The sampling region position is initially (at time  $t_0$ ) located near the upstream edge of the crab, shown at a distance  $X_0$  from the crab center in Fig. 9. To avoid shadowing and other problems, the concentration field is examined at a period  $\tau$  earlier (i.e.,  $t = t_0 - \tau$ ). The position of

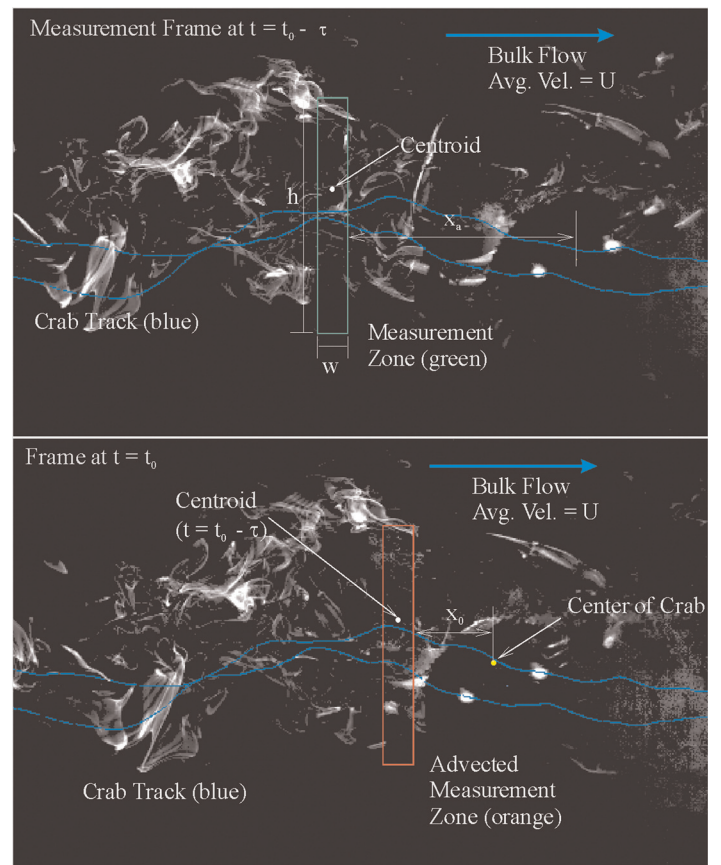


**Fig. 9.** Description of the sampling zone for evaluating the transverse signal distribution. Due to shadowing concerns, concentration data are extracted at an earlier upstream location (green box in upper panel) and assumed to be advected to the chemosensory location (orange box in lower panel). Note that the bright spots in the lower portion of the orange measurement zone are crab legs and claws, which demonstrates the challenge of extracting accurate concentration data near the crab body. The sampling region position is initially located at a distance  $X_0$  upstream of the crab center position, which corresponds to the upstream position of the crab body (shown in lower image). To evaluate the sampling region location at an earlier time ( $t_0 - \tau$ ), the sampling region is shifted upstream by the advection distance  $U\tau$ . Hence, the distance from the crab center to the sampling zone,  $X_{gr}$ , equals  $U\tau + X_0 + \Delta X_{crab}$  (shown in upper image). The streamwise width of the sampling region,  $w$ , is determined by the advection distance  $U\Delta t$  and the distance that the crab travels  $\Delta x$  between measurement samples, such that all chemosensory structure encountered by the crab between samples ( $\Delta t \approx 0.21$  s) is included. The time delay ( $\tau$ ) shown corresponds to approximately 1 s.

the sampling region at the earlier time is farther upstream due to the fact that the concentration filaments within the region are advected by the bulk flow motion during the period  $\tau$ . The crab is downstream at the earlier time and hence does not interfere with sampling of the concentration field. The concentration field is sampled at this earlier time, and the filament structure is assumed to be fixed and simply advected by the mean flow. Returning to the original reference time,  $t_0$ , the crab is in its original location and the concentration distribution is located in the original sampling region at the upstream edge of the crab.

As a simple means of quantifying the signal contrast across the crab body, we compared the transverse locations of the crab center and centroid of the concentration distribution within the sampling region. A concentration centroid location that deviates more than a threshold distance ( $\pm 0.5$  cm) from the crab center indicates a transverse bias in the chemical stimulus. We performed an autocorrelation analysis to confirm whether the transverse bias was maintained in the sampling region over the advection period. In this case, concentration fields collected without a crab present were evaluated in order to provide a sufficient number of samples ( $N = 7800$ ) for convergence of the statistical calculation and to avoid shadowing issues. The transverse bias was calculated for a sampling region and for the sampling region displaced upstream at an earlier time as described above. The data revealed that the transverse bias remained strongly correlated (correlation coefficient of approximately 0.8 or greater) for the time periods (approximately 1 s) and sampling region sizes used in this study, hence providing justification for employing the described sampling procedure (Dickman 2008).

Figs. 10 and 11 show the extracted results for two example crab tracks (labels 1364L and 465L, respectively) that relate crab center position, the centroid of the concentration distribution in the sampling region, and the animal's directional bias. In both examples, the crabs tend to respond to contrast in the concentration distribution. For example, the crab with label 1364L (Fig. 10) started near the center of the plume, received a strong signal bias toward the left between 8 and 10 s and subsequently moved toward the left (i.e., toward negative values of  $y$ ). The signal bias switched to the right between 10 and 11.5 s and the crab followed with movement to the right (starting at approximately 10.5 s). The signal bias between 12 and 14 s was again toward the left and the subsequent movement (starting at approximately 13.5 s) was to the left. Crab 465L reacted similarly (Fig. 11); the stimulus bias was initially toward the left (predominantly to the left for the time period less than 6 s) and the crab moved consistently to the left (until approximately 8 s). The signal bias was toward the right between 6 and 11 s. The crab started to move to the right at approximately 10 s. For most of tracks examined, the concentration centroid and plume centerline began to coincide as the source was approached (as shown in Fig. 10), indicating the crab was near the center of the plume. The record for crab 465L (Fig. 11) is unusual as the crab was located toward the right near to the source.

## Discussion

A major hindrance to studying chemically mediated guidance is the difficulty of establishing the relevant signal properties of chemical stimulus plumes. In auditory, visual, and lateral

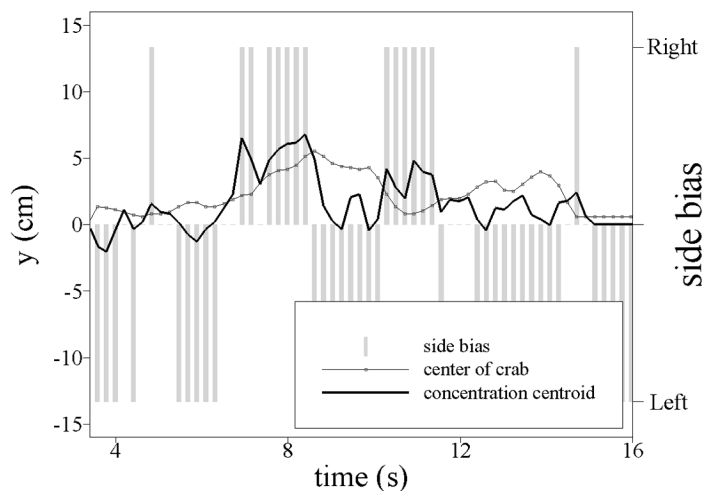


**Fig. 10.** Example time records for a successful blue crab search (crab label 1364L) comparing the crab position to the concentration distribution. The crab center is defined as the midpoint between the LEDs on the backpack and quantifies the transverse position of the crab. The concentration centroid is calculated for the sampling region described in Fig. 9. Side bias is established based on the difference between the crab position and the position of the concentration centroid. The bias is marked as left or right for differences greater than  $\pm 0.5$  cm. The crab tends to follow the transverse bias provided by the plume structure for the track shown.

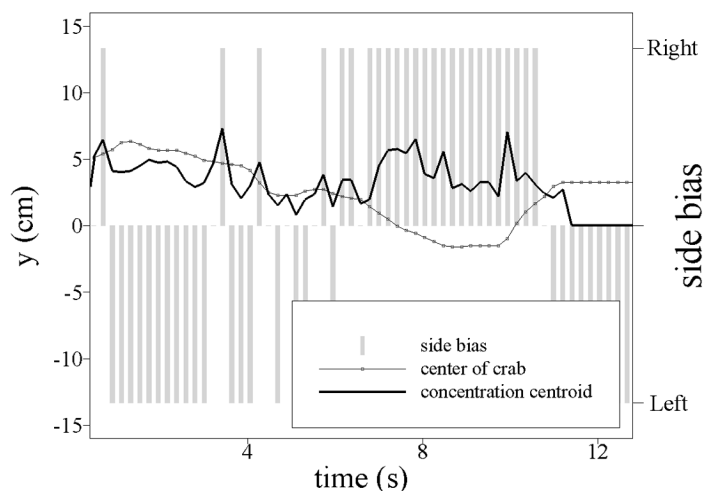


**Fig. 11.** Example time records for a successful blue crab search (crab label 465L) comparing the crab location to the concentration centroid of the sampling region described in Fig. 9. All definitions are the same as in Fig. 10. In this case, the crab loses contact with the plume at approximately  $t = 6$  s, decelerates and stops at approximately  $t = 10$  s (the stationary period appears in Fig. 8). Upstream motion resumes once the crab receives a strong bias to the right (revealed by the spike in the concentration centroid record).

line systems, relating stimulus properties (e.g., frequency, pressure) to neural and behavioral responses has led to substantial insights about sensory system function (Bradbury and Vehrencamp 1998). In contrast, the stimulus properties relevant to chemosensory systems responsible for odor-mediated guidance in turbulent odorant fields remain largely speculative. Unlike microorganisms that experience well-defined chemical gradients produced by molecular diffusion, turbulent plumes experienced by larger animals such as moths and crustaceans cannot be characterized easily (Webster and Weissburg 2009). Here, turbulent fluid motion creates spatially and temporally complex and unpredictable plumes whose features defy characterization by analytic methods (e.g., diffusion models) or numerical simulation.

Our current understanding of chemosensory organization is hindered by the complex, unpredictable, and difficult to manipulate nature of turbulent odorant plumes. As a result, we have been unable to firmly link spatial and temporal properties of chemical signal structure to resulting, specific animal movements, and the mechanisms used by this sensory system to encode information remain obscure. Establishing the stimulus patterns that result in given movements (e.g., turns, upstream movements, etc.) will help define the necessary properties of the chemosensory periphery involved in odorant-mediated guidance.

Despite various experimental challenges, meaningful data on the odorant concentration field surrounding tracking animals can be acquired from the described 3DLIF measurement technique. The measurements facilitate direct examination of the chemical stimulus near the animal to evaluate hypotheses based on previous behavior and simulation results. The three-dimensional nature of the concentration measurements is particularly important for animals such as crustaceans, due to the fact that chemical sensory organs are distributed over the body and the sensory organs move freely in all coordinate directions. Although this technique is limited to well-controlled laboratory environments, it can nonetheless furnish hypotheses about animal tracking that can lend insights into behavior in the field, provide inspiration for autonomous chemical tracking agents, or suggest fruitful avenues for physiological studies. Additionally, this technique will be useful to examine the influence of mixing regime, source size, source geometry, or release rate, etc. in mediating tracking by varying specific plume properties important for animal navigation. As noted, we have a general sense of how such variables influence tracking in some aquatic and terrestrial animals, but are unable to identify the specific changes in plume structure that are responsible.

The 3DLIF system described in this paper does have limitations on quantification of the exact chemical stimulus received by the various blue crab chemosensors. The antennules are smaller than the resolutions used in the 3DLIF system and move in and out of the LIF measurement planes.

Flows created by crab incurrents and excurrents or antennule flicking, and imprecision in the location of the antennules prevent the extraction of exact chemical concentrations impinging upon aesthetasc arrays on the antennules. To gain such detail on the antennules may require a system resolution closer to the Batchelor scale. This would result in a field of view of about 2 cm by 2 cm (see Dasi *et al.* 2007), which is insufficient to gain simultaneous information on crab movements. Exact chemical concentrations at the outer chemosensors are similarly difficult to quantify using 3DLIF due to laser reflections, shadowing, and resolution limitations associated with the appendages. Therefore, the chemical stimulus received by a tracking blue crab using a practical 3DLIF system can only estimate the concentration field actually impinging chemosensory organs. Nonetheless, as discussed below, useful information can be extracted using quantifiable estimates of the relative pattern of chemical concentration at the various chemosensory locations.

Data taken from the sampling region near the antennules of tracking blue crabs are consistent with the presumed function of the antennules in maintaining upstream progress. The height of the antennule region changes in time, which again highlights the need for three-dimensional data in order to correctly extract the stimulus characteristics underlying orientation. We observe a general connection between the presence of bursts of concentration at the antennule region and rapid upstream movement, whereas an absence of concentration bursts at the antennules was followed by a reduction in upstream walking speed.

Extracting meaningful concentration data surrounding the sensors on the leg appendages to test hypotheses about bilateral steering proved to be more difficult due to shadowing and reflection issues. The classical concept of contrast between the left and right leg chemosensors of a tracking crustacean was not always useful because blue crab body orientation with respect to the flow vector, and consequently the odorant plume, was at an angle (illustrated in Fig. 6). In many cases, the left legs were located directly upstream of the right legs, thereby corrupting a useful bilateral comparison between the left and right leg chemosensors. Nevertheless, we were able to develop a procedure to employ the sequences of three-dimensional data to examine the transverse variation of the concentration distribution just upstream of the leading legs of the tracking crab. Bias, or odorant signal asymmetry, in sampling regions upstream of the blue crab was revealed by comparing the centroid of the concentration distribution with the crab location. For the two example tracks discussed, the crabs generally followed the directional signal provided by the transverse bias in the plume structure. Thus, even though spatial asymmetry often did not correspond to the left-right body axis, blue crabs seemingly are able to use spatial patterns in the concentration field to maintain transverse position within the plume.

The process of combining behavioral studies with direct quantification of odorant stimulus is not limited to LIF. Electrodes or other sensors can be connected to tracking organisms either

externally or internally (e.g., Basil and Atema 1994). Leonard et al. (1994) implanted electrodes capable of detecting odorant concentrations at the tips of the antennules of lobsters. A concentration time record was recorded via an amplifier-transmitter backpack attached to the lobster. Vickers and Baker (1994) attached an excised antenna connected to an electroantennogram to a moth with unaltered antennae. The attached antenna required a small wire lead (1.5 m long) that traveled with the moth as it tracked a pheromone plume in a wind tunnel. Using the excised antenna apparatus, Vickers et al. (2001) recorded electrical output of pheromone stimulus simultaneously with tracking in a laboratory wind tunnel for 20 moths.

Collecting time-records at the chemosensory organs of a blue crab would require multiple sensors and some means of transmitting the data (i.e., wires) to an amplifier and recorder. Attachment of multiple sensors to a blue crab, particularly on the legs, would likely impair movement, distress the animal, and diminish tracking abilities. While the future development of minute external chemical sensors with wireless data transmission abilities in the future may resolve difficulties associated with sensors, laser-induced fluorescence avoids the wires or backpacks required for external or internal sensors. Therefore, laser-induced fluorescence, as described herein, is a good approach because it minimizes the physical limitations imposed on the tracking crab while providing a non-intrusive sampling method.

We conclude that our experimental technique is an effective method for quantifying the chemical concentration field surrounding actively tracking blue crabs and can be used for a variety of other animals (e.g., gastropods). Our data facilitate a direct comparison of the stimulus pattern with crab kinematic response. The presented (typical) data are consistent with previous hypotheses about the stimulus patterns that induce upstream motion and transverse positioning by blue crabs. We are currently performing detailed analysis to gain further insights into the stimulus patterns that mediate specific acts, the role of three-dimensional structure, and the context or history dependent changes in stimulus response patterns as crabs track towards the source.

## References

- Albertson, M. L., Y. B. Dai, R. A. Jensen, and H. Rouse. 1950. Diffusion of submerged jets. *ASCE Trans.* 115:639-664.
- Arcoumanis, C., J. J. McGuirk, and J. M. L. M. Palma. 1990. On the use of fluorescent dyes for concentration measurements in water flows. *Exp. Fluids* 10:177-180.
- Bara, B. M., D. J. Wilson, and B. W. Zelt. 1992. Concentration fluctuation profiles from a water channel simulation of a ground-level release. *Atmos. Environ. A* 26:1053-1062.
- Basil, J., and J. Atema. 1994. Lobster orientation in turbulent odor plumes: Simultaneous measurement of tracking behavior and temporal odor patterns. *Biol. Bull.* 187:272-273.
- Batchelor, G. K. 1959. Small-scale variation of convected quantities like temperature in turbulent fluid 1. General discussion and the case of small conductivity. *J. Fluid Mech.* 5:113-133.
- Brackmann, U. 2000. *Lambdachrome laser dyes*. Lambda Physik AG, Göttingen, Germany.
- Bradbury, J. W., and S. L. Vehrencamp. 1998. *Principles of animal communication*. Sinauer Associates.
- Crimaldi, J. P. 1997. The effect of photobleaching and velocity fluctuations on single-point LIF measurements. *Exp. Fluids* 23:325-330.
- . 2008. Planar laser induced fluorescence in aqueous flows. *Exp. Fluids* 44:851-863.
- and J. R. Koseff. 2001. High-resolution measurements of the spatial and temporal scalar structure of a turbulent plume. *Exp. Fluids* 31:90-102.
- , M. A. R. Koehl, and J. R. Koseff. 2002a. Effects of the resolution and kinematics of olfactory appendages on the interception of chemical signals in a turbulent odor plume. *Environ. Fluid Mech.* 2:35-63.
- , M. B. Wiley, and J. R. Koseff. 2002b. The relationship between mean and instantaneous structure in turbulent passive scalar plumes. *J. Turbul.* 3(014):1-24.
- Dasi, L. P., F. Schuerg, and D. R. Webster. 2007. The geometric properties of high Schmidt number passive scalar iso-surfaces in turbulent boundary layers. *J. Fluid Mech.* 588:253-277.
- Dickman, B. D. 2008. *Chemical and hydrodynamical cue structure in the context of turbulent odor plume tracking*. Ph.D. Thesis, Georgia Institute of Technology.
- Dinar, N., H. Kaplan, and M. Kleiman. 1988. Characterization of concentration fluctuations of a surface plume in a neutral boundary layer. *Bound.-Lay. Meteorol.* 45:157-175.
- Elkinton, J. S., R. T. Cardé, and C. J. Mason. 1984. Evaluation of time-average dispersion models for estimating pheromone concentration in a deciduous forest. *J. Chem. Ecol.* 10:1081-1108.
- Fackrell, J. E., and A. G. Robins. Concentration fluctuations and fluxes in plumes from point sources in a turbulent boundary layer. *J. Fluid Mech.* 117:1-26.
- Ferrier, A. J., D. R. Funk, and P. J. W. Roberts. 1993. Application of optical techniques to the study of plumes in stratified fluids. *Dynam. Atmos. Oceans* 20:155-183.
- Finelli, C. M., N. D. Pentcheff, R. K. Zimmer-Faust, and D. S. Wethey. 1999. Odor transport in turbulent flows: Constraints on animal navigation. *Limnol. Oceanogr.* 44:1056-1071.
- Gomez, G., and J. Atema. 1996. Temporal resolution in olfaction II: Time course of recovery from adaptation in lobster chemoreceptor cells. *J. Neurophysiol.* 76:1340-1343.
- Gulitski, G., M. Kholmyansky, W. Kinzelbach, B. Lüthi, A. Tsinober, and S. Yorish. 2007. Velocity and temperature derivatives in high-Reynolds-number turbulent flows in the atmospheric surface layer: Part 1. Facilities, methods and some general results. *J. Fluid Mech.* 589:57-81.
- Jackson, J. L., D. R. Webster, S. Rahman, and M. J. Weissburg. 2007. Bed-roughness effects on boundary-layer turbulence and consequences for odor-tracking behavior of

- blue crabs (*Callinectes sapidus*). *Limnol. Oceanogr.* 52:1883-1897.
- Jones, C. D. 1983. On the structure of instantaneous plumes in the atmosphere. *J. Hazard. Mater.* 7:87-112.
- Keller, T. A., I. Powell, and M. J. Weissburg. 2003. Role of olfactory appendages in chemically mediated orientation of blue crabs. *Mar. Ecol. Prog. Ser.* 261:217-231.
- Koehl, M. A. R. 2006. The fluid mechanics of arthropod sniffing in turbulent odor plumes. *Chem. Senses* 31:93-105.
- , J. R. Koseff, J. P. Crimaldi, M. G. McCay, T. Cooper, M. B. Wiley and P. A. Moore. 2001. Lobster sniffing: Antennule design and hydrodynamic filtering of information in an odor plume. *Science* 294:1948-1951.
- Koochesfahani, M. M., and P. E. Dimotakis. 1985. Laser-induced fluorescence measurements of mixed fluid concentration in a liquid plane shear layer. *AIAA J.* 23:1700-1707.
- Larsen, L. G., and J. P. Crimaldi. 2006. The effect of photobleaching on PLIF. *Exp. Fluids* 41:803-812.
- Leonard, A. E., R. Voigt, and J. Atema. 1994. Lobster orientation in turbulent odor plumes: Electrical recording of bilateral olfactory sampling (antennular "flicking"). *Biol. Bull.* 187:273.
- Mafra-Neto, A., and R. T. Cardé. 1994. Fine-scale structure of pheromone plumes modulates upwind orientation of flying moths. *Nature* 369:142-144.
- Mead, K. S., M. B. Wiley, M. A. R. Koehl, and J. R. Koseff. 2003. Fine-scale patterns of odor encounter by the antennules of mantis shrimp tracking turbulent plumes in wave-affected and unidirectional flow. *J. Exp. Biol.* 206:181-193.
- Moore, P. A., and J. Atema. 1991. Spatial information in the three-dimensional fine structure of an aquatic odor plume. *Biol. Bull.* 181:408-418.
- Moore, P., and J. Crimaldi. 2004. Odor landscapes and animal behavior: tracking odor plumes in different physical worlds. *J. Mar. Syst.* 49:55-64.
- Murlis, J., J. S. Elkinton, and R. T. Cardé. 1992. Odor plumes and how insects use them. *Ann. Rev. Entomol.* 37:505-532.
- Mylne, K. R. 1993. The vertical profile of concentration fluctuations in near-surface plumes. *Bound.-Lay. Meteorol.* 65:111-136.
- Rahman, S., and D. R. Webster. 2005. The effect of bed roughness on scalar fluctuations in turbulent boundary layers. *Exp. Fluids* 38:372-384.
- Schmitt, B. C., and B. W. Ache. 1979. Olfaction: Responses of a decapod crustacean are enhanced by flicking. *Science* 205:204-206.
- Smee, D. L., and M. J. Weissburg. 2006. Clamming up: Environmental forces diminish the perceptive ability of bivalve prey. *Ecology* 87:1587-1598.
- Tian, X. D., and P. J. W. Roberts. 2003. A 3D LIF system for turbulent buoyant jet flows. *Exp. Fluids* 35:636-647.
- Van Vliet, E., S. M. Van Bergen, J. J. Derksen, L. M. Portela, and H. E. A. Van der Akker. 2004. Time-resolved, 3D, laser-induced fluorescence measurements of fine-structure passive scalar mixing in a tubular reactor. *Exp. Fluids* 37:1-21.
- Vickers, N. J. 2000. Mechanisms of animal navigation in odor plumes. *Biol. Bull.* 198:203-212.
- and T. C. Baker. 1994. Reiterative responses to single strands of odor promote sustained upwind flight and odor source location by moths. *Proc. Nat. Acad. Sci. USA* 91:5756-5760.
- , T. A. Christensen, T. C. Baker, and J. G. Hildebrand. 2001. Odour-plume dynamics influence the brain's olfactory code. *Nature* 410:466-470.
- Wang, G. R., and H. E. Fiedler. 2000. On high spatial resolution scalar measurement with LIF. Part 1: Photobleaching and thermal blooming. *Exp. Fluids* 29:257-264.
- Webster, D. R., and M. J. Weissburg. 2001. Chemosensory guidance cues in a turbulent chemical odor plume. *Limnol. Oceanogr.* 46:1034-1047.
- and ———. 2009. The hydrodynamics of chemical cues among aquatic organisms. *Annu. Rev. Fluid Mech.* 41:73-90.
- , S. Rahman, and L. P. Dasi. 2001. On the usefulness of bilateral comparison to tracking turbulent chemical odor plumes. *Limnol. Oceanogr.* 46:1048-1053.
- , S. Rahman, and L. P. Dasi. 2003. Laser-induced fluorescence measurements of a turbulent plume. *J. Eng. Mech.-ASCE* 129:1130-1137.
- Weissburg, M. J. 2000. The fluid dynamical context of chemosensory behavior. *Biol. Bull.* 198:188-202.
- , and R. K. Zimmer-Faust. 1993. Life and death in moving fluids: Hydrodynamic effects on chemosensory-mediated predation. *Ecology* 74:1428-1443.
- and D. B. Dusenbery. 2002. Behavioral observations and computer simulations of blue crab movement to a chemical source in a controlled turbulent flow. *J. Exp. Biol.* 205:3387-3398.
- , C. P. James, D. L. Smee, and D. R. Webster. 2003. Fluid mechanics produces conflicting constraints during olfactory navigation of blue crabs, *Callinectes sapidus*. *J. Exp. Biol.* 206:171-180.
- Zimmer, R. K., and C. A. Butman. 2000. Chemical signaling processes in the marine environment. *Biol. Bull.* 198:168-187.
- Zimmer-Faust, R. K., C. M. Finelli, N. D. Pentcheff, and D. S. Wethey. 1995. Odor plumes and animal navigation in turbulent water flow: A field study. *Biol. Bull.* 188:111-116.

Submitted 6 June 2008

Revised 1 December 2008

Accepted 11 December 2008